Electrochimica Acta, Vol. 38, No. 5, pp. 703–715, 1993
Printed in Great Britain.

0013–4686/93 $6.00 + 0.00

A MECHANISTIC APPROACH TO THE ELECTROFORMATION OF ANODIC LAYERS ON COPPER AND THEIR ELECTROREDUCTION IN AQUEOUS SOLUTIONS CONTAINING $NaHCO_3$ AND Na_2CO_3

M. PÉREZ SÁNCHEZ, R. M. SOUTO, M. BARRERA, S. GONZÁLEZ, R. C. SALVAREZZA* and A. J. ARVIA*

Departamento de Química Física, Universidad de La Laguna, Tenerife, Spain

(*Received* 18 *June* 1992; *in revised form* 9 *September* 1992)

Abstract—The electrochemical behaviour of Cu in solutions containing $Na_2CO_3 + NaHCO_3$ ($8.8 < pH < 11.1$) has been studied using potentiodynamic and potentiostatic techniques complemented by Scanning Electron Microscopy. The initial stages of the anodic layer formation involve the electroformation of a thin inner Cu_2O layer followed by the growth of a $CuO/Cu(OH)_2$–$CuCO_3$ complex outer layer. Soluble Cu(II) species were detected in the entire anodization potential range. Kinetic models devised for phase change electrochemical processes have been applied to explain the characteristics of anodic and cathodic current transients.

Key words: Cu corrosion, Cu anodic layers, nucleation and growth processes, solution composition, Cu passivation.

1. INTRODUCTION

The electrochemical behaviour of Cu in moderate alkaline media has been widely studied both in plain NaOH and in salt-containing solutions at different pH[1–10]. Cu passivation in plain NaOH solutions was described through two main processes, namely, the initial formation of the Cu_2O monolayer followed by the growth of a massive Cu_2O layer, and the build-up of the CuO–$Cu(OH)_2$ layer, the overall process being accompanied by the formation of Cu(I) and Cu(II) soluble species[7–9]. Accordingly, the anodic layer consisted of a complex layer involving initial reactions leading to a Cu/Cu_2O (porous inner layer) structure and further growth of a Cu/Cu_2O (porous inner layer)/$CuO/Cu(OH)_2$ structure was advanced[7, 8]. It was also found that the relative contribution of the two main processes and the structure of the passive layer depended on a number of variables, such as the potential routine employed in the experiments, the solution composition, the Cu surface treatment and the temperature[7–9, 11–13].

The protective properties of the anodic layer produced on Cu in alkaline solutions vary strongly with the nature of anions in the solution[13–15]. Thus, in aqueous solutions containing either a carbonate[13] or a phosphate salt[15] the protective properties of the anodic layer could be improved, although this effect depends considerably on the pH, the relative concentration of anions in the solution and the solubility product of the corresponding Cu salts. Occasionally, as occurs in alkaline solutions containing either carbonate[13] or phosphate salts[15], insoluble Cu salts become a part of the anodic layer. Conversely, the high solubility of Cu salts could favour a more extensive attack of Cu eventually leading to pitting corrosion[8, 13, 16–20]. Nevertheless, whether the anodic layer produced on Cu behaves as either a protective or a non-protective layer depends not only on its chemical composition but also on its compactness and adhesion to the Cu substrate. These two properties are closely related to the kinetics and mechanism of the growth of new phases entering the anodic layer formation[7, 8].

Voltammetric data of Cu in moderate alkaline solutions[13, 20] suggest that the main characteristics of the passivating layer could be accounted for through a composed-type passivating layer structure as that already referred to above. However, for the anodization of Cu in $NaHCO_3$ and Na_2CO_3 aqueous solutions, SEM and Electron Microprobe Analysis data indicated that Cu carbonates participate in the formation of the anodic layer structure from the very beginning of the reaction in different ways depending on the HCO_3^- ion concentration. Thus, at high positive potentials and low HCO_3^- ion concentrations Cu pitting could be promoted[13, 20]. However, the precipitation of Cu(II) carbonates in the pits hindered pit stabilization and growth[13, 20]. Otherwise, in solutions containing Cl^- ions the HCO_3^- ion acted as a pitting inhibitor shifting the breakdown potentials obtained in solutions containing the Cl^- ion to more positive potentials[20].

The following aspects of the electrochemistry of Cu in $NaHCO_3 + Na_2CO_3$ aqueous solutions at different pH ($8.8 < pH < 11.1$) are reported in this work: (i) the identification of the anodic and cathodic processes; (ii) the influence of stirring on Cu corrosion and passivation in those media; (iii) the participation of CO_3^{2-} and HCO_3^- ions in the formation of soluble Cu(II) species; (iv) the probable

* Visiting Professor, INIFTA, Universidad Nacional de La Plata, La Plata, Argentina.

mechanisms related to the formation and to the disappearance of solid phases related to Cu corrosion and passivation; and (v) the comparative behaviour of Cu in different aqueous electrolytes.

2. EXPERIMENTAL

A conventional three-electrode electrochemical cell was used. Working electrodes consisted of flat Cu discs (0.3 cm dia.) prepared from electrolytic Cu rods. Two types of specimens (i) and (ii), were used as working electrodes: (i) mechanically mirror-polished Cu specimens with fine-grained (silicon carbide) emery papers ranging from 30 to 5 μm grit, rinsed with distilled water, and finally dried in air; (ii) thermally treated Cu specimens annealed at 500°C for 2 h under a few mm pressure Ar gas to eliminate residual mechanical stresses[15]. These specimens were electropolished in aqueous 85% H_3PO_4 at 0.3 A cm^{-2} for 5–10 min at room temperature, then rinsed thoroughly with distilled water, and finally dried under Ar. Thermally treated and electropolished Cu specimens provided the most reproducible electrochemical data.

Each Cu specimen was axially mounted at the extreme of the shaft of a rotating disc electrode device so that the contact between the Cu disc surface and the solution was made through a hanging meniscus-disc-electrode arrangement[21, 22]. The potential of the working electrode was measured against a NaCl(saturated)-calomel electrode (*ssce*). A cylindrical Pt grid was used as counter electrode.

Solutions were prepared from twice-distilled water and A.R. chemicals, and purged with Ar. The entire electrochemical system was run continuously under Ar. The following solutions were employed in the present work, $(0.1-x)$ M $NaHCO_3 + x$ M Na_2CO_3 for $x = 0$, 0.01, 0.03, 0.05, 0.07 and 0.1 ($8.8 < pH < 11.1$). To establish possible specific effects of anions, experiments in 0.075 M $Na_2B_4O_7$ + 0.15 M H_3BO_3 buffer (pH = 9.0) and in 0.075 M $Na_2B_4O_7$ + 0.15 M $H_3BO_3 + y$ M $NaHCO_3$ ($y = 0.01$ and 0.1) were also performed.

A new Cu specimen was used for each run. Firstly, the working electrode was potential cycled at 0.01 V s^{-1} from $E_{sc} = -0.80$ V to $0.35 \leqslant E_{sa} \leqslant 0.80$ V, depending of the solution composition. Conventional single sweep and repetitive voltammograms, current/potential curves under working electrode rotation, and potentiostatic current transients under different conditions were recorded using conventional circuitries. All runs were performed at 25 ± 0.1°C.

3. RESULTS AND INTERPRETATION

3.1. *Voltammetric data*

3.1.1. *General features.* Cyclovoltammograms were run with Cu specimens of both types: (i) and (ii) at various pH, potential sweep rates (v) and anodic (E_{sa}) and cathodic (E_{sc}) switching potentials to establish the potential ranges of the different electrochemical reactions of Cu in the working solutions and their kinetic characteristics, and to select the most adequate conditions for the potentiostatic investigation of either the electroformation of corrosion and passivating products or their electroreduction reactions. The voltammograms became highly dependent on pH, solution composition, E_{sa}, E_{sc} and duration of the potential cycling.

The cyclovoltammograms of Cu in 0.1 M $NaHCO_3$ (pH 8.8) and in 0.05 M $NaHCO_3$ + 0.05 M Na_2CO_3 (pH 9.8) (Fig. 1) are qualitatively comparable. During the potential cycling the voltammetric charges relating to peaks II_a, I_c and II_c become particularly enhanced. Trends in the change of the different peaks are indicated by the arrows in Fig. 1. After a certain number of cyles, which depends on solution pH and switching potentials, the stabilized voltammograms are attained for all solutions used in this work (Fig. 2). These voltammograms show a cathodic current baseline related to the electrodeposition of soluble Cu(II) which has been formed during the repetitive scans. The magnitude of this current depends on both the applied potential routine and the Cu electrode pretreatment.

Peaks I_a and II_a are related to the formation of Cu_2O and CuO, respectively, as in plain NaOH solutions[11]. When E_{sa} is set above 0.0 V an anodic

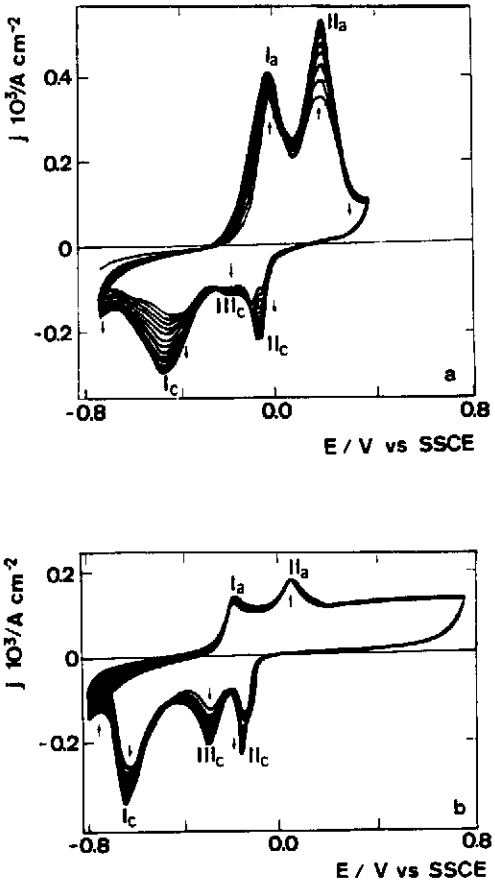

Fig. 1. Cyclovoltammograms resulting for Cu specimens (type i) at 0.01 V s^{-1}: (a) 0.1 M $NaHCO_3$, pH 8.8; (b) 0.05 M $NaHCO_3$ + 0.05 M Na_2CO_3, pH 9.8; 25°C. The arrows indicate the trend of the voltammograms to reach the stabilized current–potential profiles.

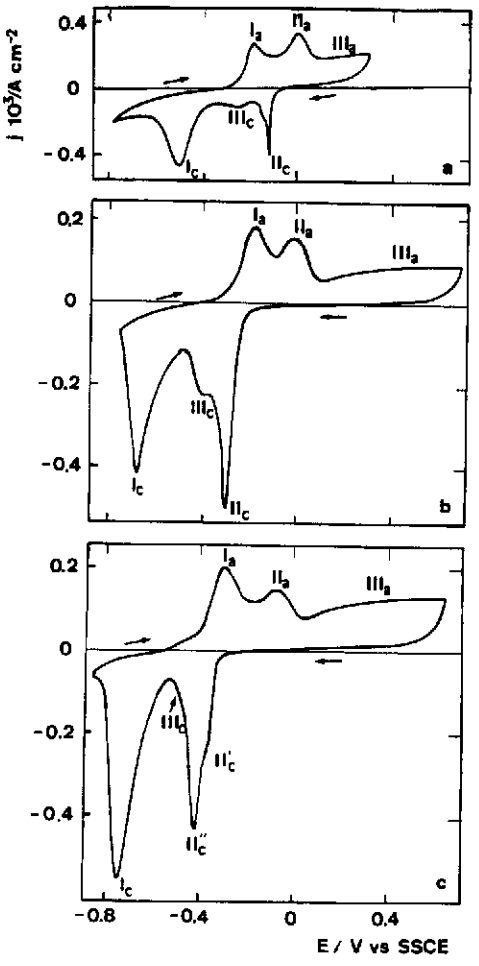

Fig. 2. Voltammograms run with Cu specimens (type i) at 0.01 V s^{-1}; (a) 0.1 M $NaHCO_3$, pH 8.8; (b) 0.07 M $NaHCO_3$ + 0.03 M Na_2CO_3, pH 9.8; (c) 0.1 M Na_2CO_3, pH 11.1. 25°C.

current plateau (III_a) extending up to 0.40 V can be observed. The reverse potential scan shows three cathodic peaks (I_c, II_c and III_c) instead of two peaks found in plain NaOH solutions. Peak II_c is a complex peak involving the contributions of peaks II'_c and II''_c, the relative height of these peaks changing with both potential cycling time and E_{sa}. The appearance of peak III_c is enhanced as E_{sa} is set in the current plateau (III_a) region. Peak III_c has been assigned to the electroreduction of the Cu carbonate–Cu hydroxide layer formed at potentials more positive than 0.0 V[13], whereas peaks II_c and I_c have been associated with the electroreduction of CuO–$Cu(OH)_2$ to Cu_2O, and Cu_2O to Cu, respectively.

The potentials of the anodic (I_a and II_a) and the cathodic (I_c and II_c) peaks shift linearly with pH. These dependences are given through the following slopes, $\Delta E_{p,Ia}/\Delta pH = \Delta E_{p,IIa}/\Delta pH = -0.05 \pm 0.01$ V/pH unit, and $\Delta E_{p,Ic}/\Delta pH = \Delta E_{p,IIc}/\Delta pH = -0.120 \pm 0.015$ V/pH unit, where $E_{p,i}$ stands for the potential of current peak i ($i = I_a, I_c, II_a, II_c$). The pH dependences of $E_{p,Ia}$ and $E_{p,IIa}$ approach the predictions of Nernst equations for Cu/Cu_2O and Cu_2O/CuO reactions at equilibrium, respectively[2]. For peak III_c no clear-cut pH dependence could be determined. The shift of peaks I_c and II_c with pH makes peak III_c appear as a separate peak located between peaks II_c and I_c at the lowest pH (Fig. 2a).

At constant pH, the single sweep voltammograms for a Cu specimen (type ii) in 0.1 M $NaHCO_3$, pH 8.8, run by changing E_{sa} stepwise positively, show the following features: (i) both peaks I_c and II_c move negatively as expected for a progressive contribution of ageing processes at the anodically-formed product layer[23]; (ii) peak III_c can be detected when E_{sa} exceeds the potential range of peak II_a; (iii) peaks II_a and I_a are largely overlapped; (iv) the single sweep voltammetric condition and $E_{sa} < 0.40$ V makes the cathodic current baseline appear extremely small. Furthermore, the rotation of the Cu specimens results in the increase of the anodic current recorded from −0.20 V upwards, the decrease of the cathodic to anodic voltammetric charge ratio, and the positive shift of $E_{p,Ic}$ and $E_{p,IIc}$[13].

A series of voltammograms were run with Cu specimens (type ii) starting the first positive going potential scan in still solution, and commencing the working electrode rotation at $\omega = 1000$ rpm during the reverse scan from 0.20 V downwards (Fig. 3). In these cases, stirring at point A produces a sudden anodic current jump attaining a plateau which covers the 0.20–0.0 V range. Below 0.0 V the anodic current decreases and later at −0.18 V changes over to a cathodic current. The negative going potential scan shows a considerable decrease in the height of peak I_c, and the absence of peaks II_c and III_c. The second cyclovoltammogram run from −0.80 V upwards displays an anodic current plateau covering the potential range of peak I_a, and partially that of peak II_a. Furthermore, a near linear anodic current

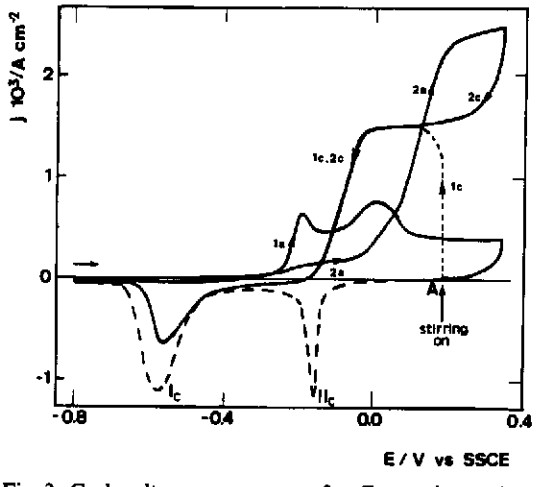

Fig. 3. Cyclovoltammograms run for Cu specimens (type ii); 0.1 M $NaHCO_3$; 25°C. The voltammetric sweep commences at −0.8 V. The sequence of the sweeps is: 1a (quiescent solution); 1c; 2a; and 2c (under stirring at 1000 rpm). Stirring was started when the potential sweep reached point A. The dashed line corresponds to the cathodic profile in the absence of stirring.

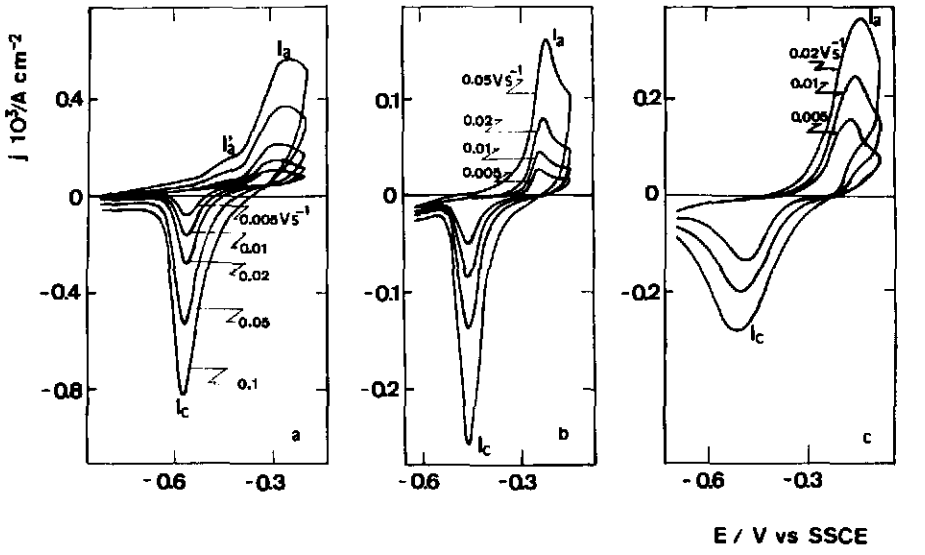

Fig. 4. Stabilized voltammograms resulting for Cu specimens (type i) in the potential region of Cu(O)/Cu(I) redox system at different v values as indicated in the figures: (a) 0.1 M Na_2CO_3, pH 11.1; (b) 0.05 M $NaHCO_3$ + 0.05 M Na_2CO_3, pH 9.8; (c) 0.1 M $NaHCO_3$, pH 8.8; 25°C.

increase in the −0.02 to 0.06 V range followed by a steep increase up to a current plateau covering from *ca.* 0.25 V to E_{sa} can be observed. The subsequent reverse voltammogram shows a current loop with a crossing potential at *ca.* 0.12 V, and afterwards the voltammogram tends to coincide with the previous one.

According to the preceding results stirring promotes Cu corrosion in the Na_2CO_3–$NaHCO_3$ solution probably because the formation of the outer part of the anodic layer is largely impeded. As seen through peak I_c, apparently a part of the inner anodic layer, *ie* the Cu_2O layer remains on the Cu substrate even under stirring.

3.1.2. *Conjugated redox couples.* Voltammograms run by adequately setting E_{sa} and E_{sc} allow to identify the conjugated pair of peaks related to the Cu/Cu_2O (Fig. 4) and the Cu_2O/CuO (Fig. 5) redox reactions at different pH.

The electro-oxidation of Cu to Cu(I) in 0.1 M Na_2CO_3 (Fig. 4a) implies the initial formation of a $Cu(OH)_{ad}$ precursor (hump I'_a) at a potential slightly

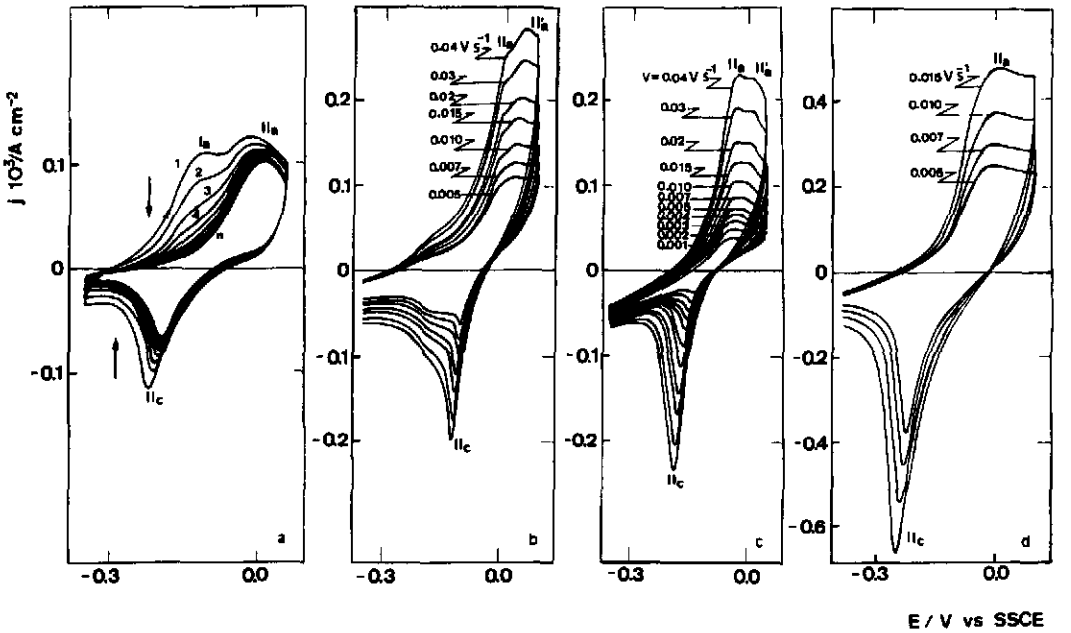

Fig. 5. (a) Stabilization of the voltammograms obtained on Cu specimens (type ii) at 0.01 V s^{-1} in the potential range of peaks II_a and II_c in 0.1 M $NaHCO_3$, pH 8.8. (b)–(d) Stabilized voltammograms resulting in the potential region of Cu(I)/Cu(II) redox system at different v values in (b) 0.1 M $NaHCO_3$, pH 8.8; (c) 0.05 M $NaHCO_3$ + 0.05 M Na_2CO_3, pH 9.8; and (d) 0.1 M Na_2CO_3, pH 11.1. 25°C.

lower than the reversible potential of the Cu(O)/Cu(I) system, followed by the appearance of Cu_2O when the potential of hump I'_a is exceeded[11]. Comparable results are obtained for the 0.5 M Na_2CO_3 + 0.5 M $NaHCO_3$ (Fig. 4b) and 0.1 M $NaHCO_3$ (Fig. 4c) solution, although in these cases hump I'_a appears poorly defined.

Parametric relationships for $j_{p,i}$ and $E_{p,i}$ could be established at different values of v, where $j_{p,i}$ stands for the apparent peak current density values for $i = I_a$, I_c, II_a and II_c. For 0.05 M $NaHCO_3$ + 0.05 M Na_2CO_3, a linear $\ln j_{p,I_a}$ vs. $\ln v$ plot with a slope equal to 0.8 ± 0.03 was found. Similar plots were obtained for peak I_c although in this case the slope changes from 0.5 ± 0.03 for 0.1 M Na_2CO_3 to 0.8 ± 0.03 for 0.1 M $NaHCO_3$. The dependence of E_{p,I_a} on v changes with the solution composition. Thus, in either 0.1 M Na_2CO_3 (pH 11.1) or 0.1 M $NaHCO_3$ (pH 8.8) no definite dependence E_{p,I_a} on v could be established due to the somewhat poor quantitative reproducibility of the Cu(O)/Cu(I) reaction. Otherwise, in 0.05 M $NaHCO_3$ + 0.05 M Na_2CO_3 (pH 9.8), a linear decrease of E_{p,I_a} with $\ln v$ is approached with a slope close to 0.01 V decade^{-1}; whereas E_{p,I_c} behaves practically independent of v in the $5 \times 10^{-3} \leqslant v \leqslant 0.1\,V\,s^{-1}$ range. These parametric relationships, however, become influenced by the local change of pH and the ageing processes at the anodic layer itself[23, 24].

For further investigating the conjugated pair of peaks related to the Cu(I)/Cu(II) reactions, a potential cycling was first performed until the contribution of peak I_a in the voltammogram was practically cancelled (Fig. 5a), and later, the values of E_{sc} and E_{sa} were set to cover the potential range of the Cu(I)/Cu(II) reaction. The stabilized voltammograms run at different v and pH values (Fig. 5b–d) show that the electro-oxidation of Cu_2O to $CuO/Cu(OH)_2$ in these solutions becomes also a complex process comprising of two largely overlapping peaks. Peak II'_a is not observed at the highest pH, but it is clearly displayed in 0.1 M $NaHCO_3$ (pH 8.8) (Fig. 5b). The dependence of peak II'_a on v becomes greater than that observed for peak II_a. Thus, as v is increased from 0.001 to 2 V s^{-1} the II'_a/II_a peak height ratio increases with v, the greater this increase, the lower the solution pH. At the lowest pH and $v = 0.50\,V\,s^{-1}$ both peaks are approximately equal; at $v = 2.00\,V\,s^{-1}$, peak II'_a is higher than peak II_a, and finally, at $v > 2\,V\,s^{-1}$ both peaks are no longer observed.

A linear $\ln j_{p,II_a}$ vs. $\ln v$ plot with a slope *ca.* 0.63 ± 0.03 for 0.1 M Na_2CO_3 (pH 11.1) was obtained; whereas two linear portions could be distinguished in both 0.1 M $NaHCO_3$ (pH 8.4) and in 0.05 M $NaHCO_3$ + 0.05 M Na_2CO_3 (pH 9.8), the corresponding slopes being 0.50 ± 0.02 ($10^{-3} \leqslant v \leqslant 10^{-2}\,V\,s^{-1}$ range), and 0.60 ± 0.03 ($0.02 \leqslant v < 0.1\,V\,s^{-1}$ range). On the other hand, for all solutions two linear portions in the $\ln j_{p,II_c}$ vs. v plots were displayed, the corresponding slopes being 0.42 ± 0.03 ($0.02 \leqslant v \leqslant 0.1\,V\,s^{-1}$ range), and 0.60 ± 0.03 ($10^{-3} \leqslant v \leqslant 7 \times 10^{-3}\,V\,s^{-1}$ range) for 0.1 M Na_2CO_3 and 0.05 M $NaHCO_3$ + 0.05 M Na_2CO_3; and 0.58 ± 0.03 and 0.85 ± 0.03 for 0.1 M $NaHCO_3$. Besides, a linear E_{p,II_a} vs. $\ln v$ plot with a slope close to $RT/2F$ is only seen for 0.1 M Na_2CO_3. The plot E_{p,II_c} vs. $\ln v$ behaves similarly to that described for peak II_a.

3.1.3. *The influence of* $NaHCO_3$ *addition on the behaviour of* Cu *in borate buffer.* The voltammograms of Cu specimens (type ii) in a borate buffer run at 0.01 V s^{-1} covering the −0.80 to 0.80 V range (Fig. 6) show a broad anodic peak containing peaks I_a and II_a followed by another broad peak III_a[8]. The reverse scan exhibits peak II_c and I_c. In this case the electrode rotation up to $\omega = 1000$ rpm has no significant influence on the voltammogram.

Similar voltammograms run in borate buffer + 0.01 M $NaHCO_3$ for $\omega \leqslant 500$ rpm show that both the base anodic and cathodic currents increase with ω (Fig. 6b). In these voltammograms a distinction among peaks I_a, II_a and III_a can also be made although peak I_a largely overlaps peak II_a. The reverse scan exhibits an anodic current down to *ca.* −0.08 V, *ie* about 0.17 V more negative than the reversible potential of Cu(II)/Cu(O) redox couple. In contrast to the overall cathodic charge, under rotation up to about $\omega = 500$ rpm, the overall anodic charge is considerably increased. At $\omega > 500$ rpm the

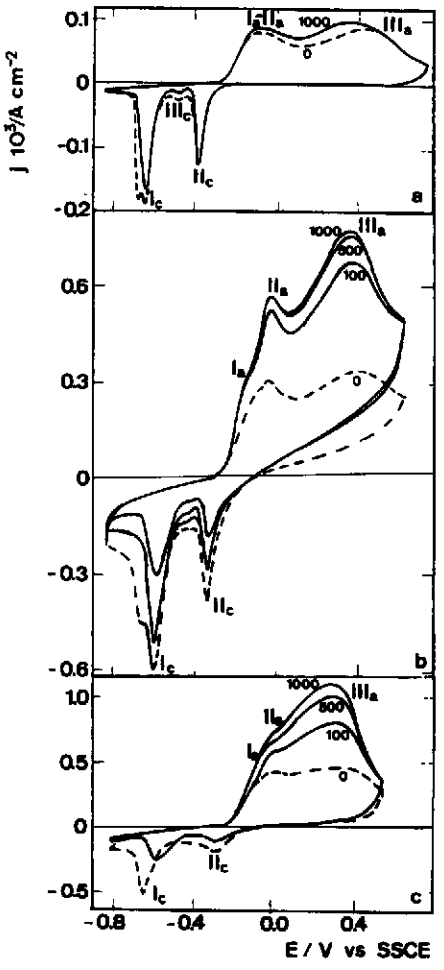

Fig. 6. Stabilized voltammograms run for Cu specimens (type ii) at 0.01 V s^{-1}, measured at different rotation speeds in rpm; 25°C: (a) borate buffer; (b) borate buffer + 0.01 M $NaHCO_3$; (c) borate buffer + 0.1 M $NaHCO_3$.

influence of rotation on the electrochemical process tends to disappear. But in all cases, in the negative going potential scan, the crossover potential related to the anodic to cathodic current change remains the same, *ie* −0.08 V.

The influence of stirring on the voltammograms can be enhanced by increasing the $NaHCO_3$ concentration in the borate buffer (Fig. 6c). In this case a situation can be reached for which the heights of peaks I_c and II_c become independent of ω, the corresponding peak potentials being positively shifted.

When the voltammogram is initiated from E_{sc} upwards with a quiescent solution, and as the value of E_{sa} is reached, stirring at $\omega = 1000$ rpm is started, the reverse voltammetric scan displays an anodic current up to the crossover potential value (Fig. 7). Further on, the rest of the voltammogram shows peaks I_c and II_c, the corresponding charges being appreciably diminished as compared to those resulting in still solution. Likewise, a considerable increase of the cathodic current baseline related to the electroreduction of soluble Cu(II) species can be noted. These results demonstrate that in the presence of $NaHCO_3$ the increase in the anodic current produced throughout stirring is related to an enhancement of the Cu electrodissolution current. However, the dissolution of the anodic layer caused by the presence of HCO_3^- ions reaches a limit for $\omega \geqslant 500$ rpm. Thence, the cathodic charge related to peaks II_c and III_c can be considered as a measure of the amount of anodic layer formed under those circumstances.

On the other hand, the dissolution of the anodic layer in solutions containing HCO_3^- produces a local acidification at the interface which is reflected in the positive potential shifts of peaks I_c and II_c (Figs 3 and 7). This effect is somewhat mitigated by the presence of the borate solution.

The preceding results definitely point out that the magnitude of the baseline cathodic current resulting for Cu specimens in $NaHCO_3 + Na_2CO_3$ solutions depends on the amount of soluble Cu(II) species present in the solution, on E_{sa}, v and cycling time.

3.2. *Potentiostatic current transients*

3.2.1. *Anodic current transients.* The anodic current transients were obtained by setting the potential at different E_s values located in the potential range of either peak I_a or peak II_a. According to the purpose of the experiments, each Cu specimen was first held 3 min at a potential E_c ($E_c < E_s$) to assure the electroreduction of the anodic layer either to Cu or to Cu_2O. Subsequently, the potential was stepped to E_s, to build up anodic products, and the current transient was recorded simultaneously (Fig. 8). Similar runs were also made at different pH values. In all cases the current transients exhibit an initial current jump followed by a continuous current decrease to approach a constant residual value.

3.2.2. *Cathodic current transients.* The following potential routine was applied for recording the cathodic current transients. Each Cu specimen was first held 3 min to E_c ($E_c > E_s$) to assure the electroreduction of the anodic layer. Subsequently, the potential was stepped to E_s, a potential within the

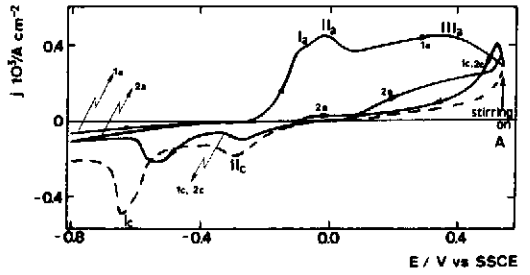

Fig. 7. Cyclovoltammograms run for Cu specimens (type ii); borate buffer + 0.1 M $NaHCO_3$; 25°C. The voltammetric sweep commences at −0.8 V. The sequence of the sweeps is: 1a (quiescent solution); 1c; 2a; and 2c (under stirring at 1000 rpm). Stirring was started when the potential sweep reached point A. The dashed line corresponds to the cathodic profile recorded in the absence of stirring.

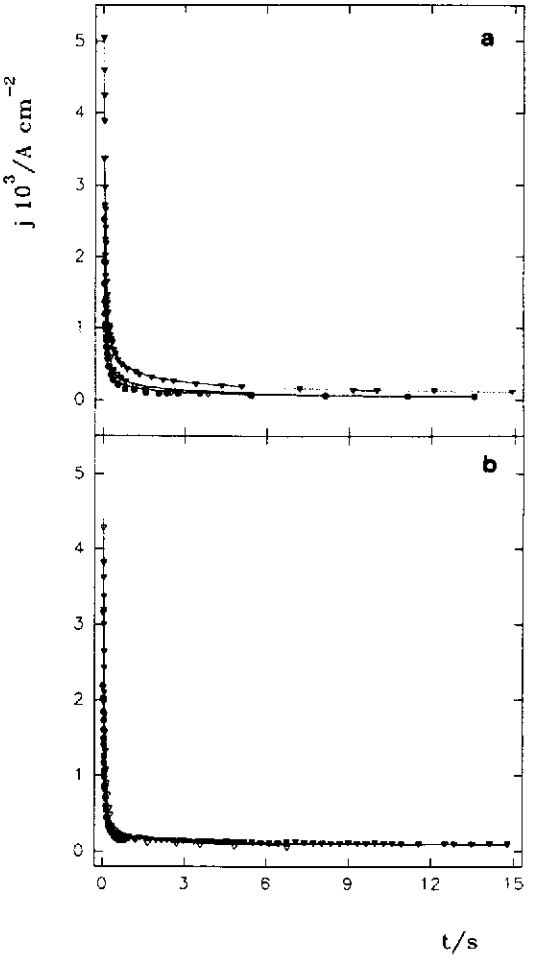

Fig. 8. Anodic current transients recorded under different experimental conditions: (a) values of E_s set in the potential range of peak I_a; (●) pH 8.8, $E_s = -0.13$ V, (▽) pH 9.8, $E_s = -0.16$ V, (▼) pH 11.1, $E_s = -0.21$ V; (b) E_s values set in the potential range of peak II_a; (●) pH 8.8, $E_s = 0.20$ V, (▽) pH 9.8, $E_s = 0.06$ V, (▼) pH 11.1, $E_s = 0.05$ V. The symbols denote the experimental data and the lines correspond to the current transients calculated with equations (8)–(10).

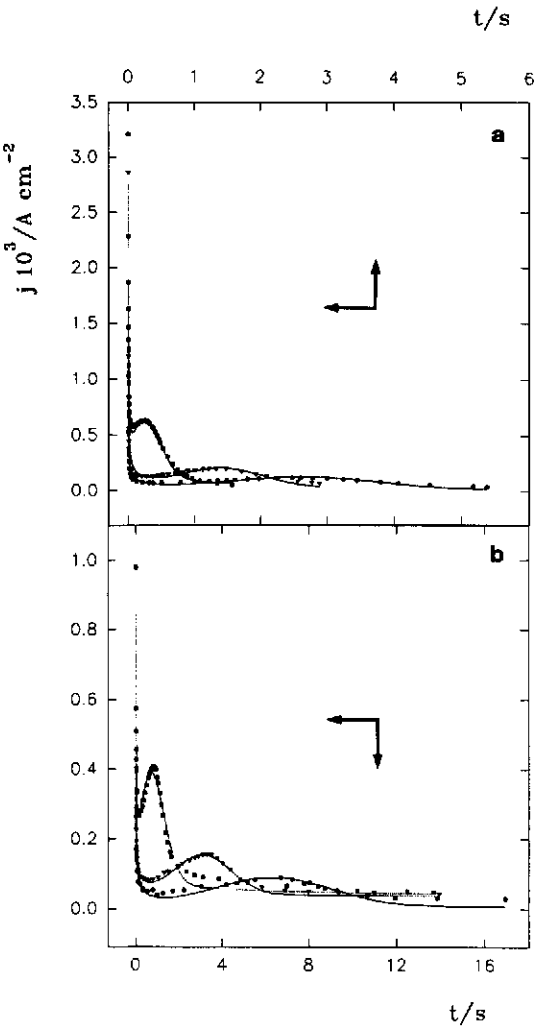

Fig. 9. Cathodic current transients recorded under different experimental conditions: (a) 0.1 M $NaHCO_3$, pH 8.8, E_a = 0.12 V for 100 s and the following E_c values, (●) −0.13 V, (▽) −0.16 V, (▼) −0.23 V; (b) 0.1 M Na_2CO_3, pH 11.1, E_a = 0.01 V for 100 s and the following E_c values (●) −0.18 V, (▽) −0.20 V, (▼) −0.25 V. 25°C.

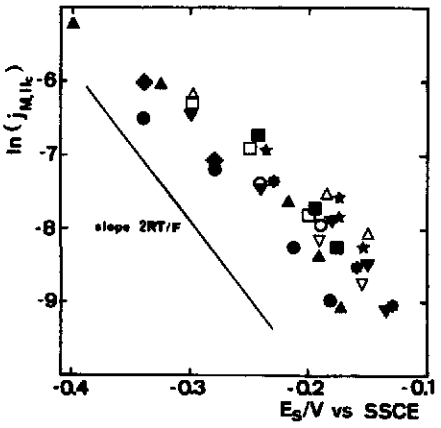

Fig. 10. Ln $j_{M,IIc}$ vs. E_s plot related to the cathodic current transients after correction for the residual current. Symbols correspond to the following experimental conditions: 0.1 M $NaHCO_3$; (○) E_a = 0.104 V, t_a = 50 s; (▽) E_a = 0.104 V, t_a = 100 s; (▼) E_a = 0.106 V, t_a = 100 s; (✱) E_a = 0.122 V, t_a = 100 s; (★) E_a = 0.250 V, t_a = 100 s; (●) E_a = 0.495 V, t_a = 100 s; 0.05 M $NaHCO_3$ + 0.05 M Na_2CO_3, (△) E_a = 0.063 V, t_a = 100 s; (▲) E_a = 0.304 V, t_a = 100 s; 0.1 M Na_2CO_3, (□) E_a = 0.0 V, t_a = 50 s; (■) E_a = 0.01 V, t_a = 100 s; (◆) E_c = 0.25 V, t_a = 100 s. The straight line indicates the reference slope $2RT/F$.

anodic current plateau (III_a) for growing the anodic layer during 100 s. Finally, the electroreduction current transients were run at a preset E_c value. The latter was set within the potential range of peak II_c. The values of E_c and E_a were adequately chosen according to the composition of the solution.

The cathodic current transients show an initial cathodic current decrease approaching a linear j vs. $t^{-1/2}$ relationship, and then a current increase up to a maximum value (j_M) at time t_M, and finally a monotonous decrease to attain a small value (Fig. 9). The value of j_M increases and the value of t_M decreases as E_c is shifted negatively. The values $\ln j_{M,IIc}$, after correction for the current baseline corresponding to each experiment (j_r), plotted against E_c (Fig. 10) approach a straight line with a slope close to $2RT/F$ for $E_c \geqslant 0.25$ V. This behaviour is also observed when either E_a or t_a is fixed as the independent variable in the experiment. Data displayed in Fig. 10 suggest a change in the kinetics of the electroreduction reaction as E_c is moved negatively.

3.3. *SEM micrographs*

In all cases the SEM micrographs after the electrochemical treatment exhibit Cu surfaces coated by non-uniform corrosion products layers (Fig. 11a, b). The film exhibits crystalline nodules whose density seemingly decreases as the pH is increased. For mechanically polished Cu specimens in contact with 0.1 M $NaHCO_3$ the scratches disappear at uncoated surface patches (Fig. 11a), but they are clearly observed in 0.1 M Na_2CO_3 (Fig. 11b). These results reveal that the depth of the localized attack increases as the pH of the solution is decreased. The SEM micrographs obtained in 0.5 M $NaHCO_3$ + 0.5 M Na_2CO_3 (Fig. 11c) shows a Cu surface partially coated by corrosion products. In this case the precipitate resembles that obtained on the Cu surface oxidized in a similar electrolyte for 20 min at 0.8 V which has been attributed to malachite[20].

The SEM micrographs of specimens cycled in the I_a–II_a and I_c–II_c potential ranges in 0.1 M Na_2CO_3 (Fig. 11d), show a crystalline precipitate which can be assigned to Cu hydroxide[25].

4. DISCUSSION

The electrochemical behaviour of Cu in aqueous solutions containing CO_3^{2-} and HCO_3^- ions[13] comprises the anodic formation of the inner Cu_2O layer (peak I_a) followed by the electroformation of an outer layer (peak II_a) involving $CuO/Cu(OH)_2$ and basic Cu carbonates. The $Cu(OH)_2$/basic Cu carbonates ratio depends on both the solution composition and the applied anodic potential routine.

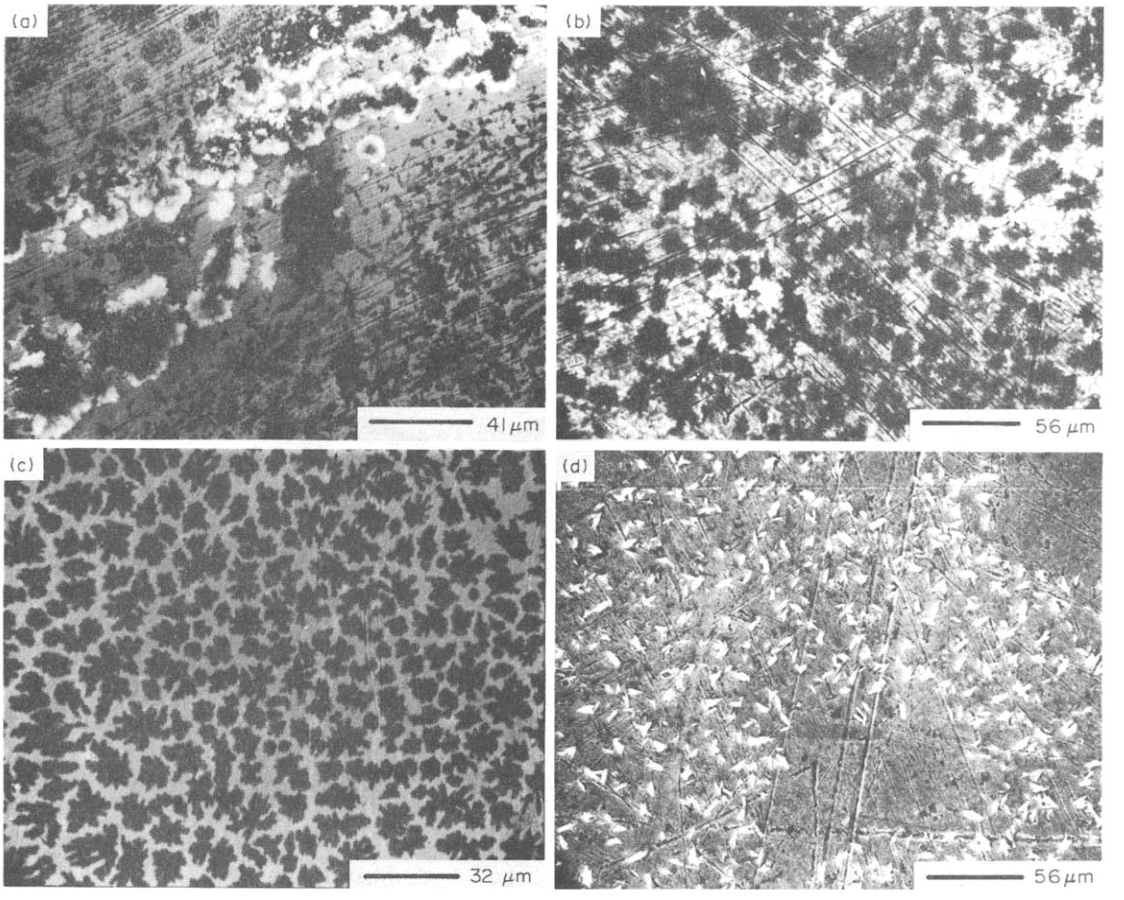

Fig. 11. SEM micrographs of Cu specimens (type i) which have been subjected to a potential cycling between E_{sc} and E_{sa} at 0.01 V s^{-1}: (a) 0.1 M $NaHCO_3$, pH 8.8, $E_{sc} = -0.75$ V, $E_{sa} = 0.35$ V; (b) 0.1 M Na_2CO_3, pH 11.1, $E_{sc} = -0.75$ V, $E_{sa} = 0.50$ V; (c) 0.05 M $NaHCO_3$ + 0.05 M Na_2CO_3, pH 9.2, $E_{sc} = -0.75$ V, $E_{sa} = 0.55$ V; (d) 0.1 M Na_2CO_3, $E_{sc} = -0.40$ V, $E_{sa} = 0.0$ V. The bars indicate the scale in micrometers.

The voltammograms systematically show that q_{1a}, the anodic charge of peak I_a, exceeds q_{1c}, the cathodic charge of peak I_c (Figs 3, 6 and 7). Therefore, only a part of the anodic charge appears as Cu_2O layer, and the difference $\Delta q_a = q_a - q_c$ results in the formation of soluble Cu(II) species. The baseline cathodic current extending from $E_{rev} = (0.299 - 0.059\,pH)$ to E_{sc}, and the residual current observed in the cathodic current transients (Fig. 9) correspond to the electroreduction of soluble Cu(II) species. The contribution of the latter gradually increases as E_{sa} is shifted positively. This means that the Cu(II) soluble species originates in the same potential range where reactions yielding Cu_2O, and $CuCO_3$ and basic $CuCO_3$ takes place.

The early formation of $CuCO_3$ in the anodization of Cu in $NaHCO_3 + Na_2CO_3$ solutions has been concluded from Electron Microprobe Analysis data[13], and it can proceed immediately after the initial Cu electro-oxidation process. The global reactions can be represented as follows

$$Cu + H_2O = Cu(OH)_{ad} + H^+ + e^-, \quad (1a)$$

$$Cu(OH)_{ad} + HCO_3^- = CuCO_3 + H_2O + e^-, \quad (1b)$$

or

$$2Cu + H_2O = Cu_2O + 2H^+ + 2e^-, \quad (2a)$$

$$Cu_2O + 2HCO_3^- = 2CuCO_3 + H_2O + 2e^-, \quad (2b)$$

followed by the formation of Cu(II) soluble species according to[20]:

$$CuCO_3 + HCO_3^- = [Cu(CO_3)_2]^{2-} + H^+. \quad (3)$$

At pH 8 the stable forms of Cu are Cu_2O and $CuCO_3$ (malachite), the relative amount of these substances depending on the concentration of HCO_3^- ions. There is no evidence that an appreciable amount of soluble Cu(II) species could be formed through a disproportionation reaction involving Cu(I) species resulting in the first electro-oxidation reaction.

As the potential increases further the formation of $Cu(OH)_2$ (peak II_a) takes place yielding basic Cu(II) carbonates according to reactions such as:

$$Cu_2O + HCO_3^- + H_2O = [Cu(OH)_2 \cdot CuCO_3] \quad \text{(malachite)} + H^+ + 2e^-, \quad (4a)$$

$$3Cu_2O + 2HCO_3^- + H_2O = 2\,[Cu(OH)_2 \cdot 2CuCO_3]\ \text{(azurite)} + 2H^+ + 2e^- \quad (4b)$$

The composition of the Cu(II) basic carbonate layer should depend on the pH of the solution. The stability constants of malachite $[CuCO_3 \cdot Cu(OH)_2]$ and azurite $[2 \cdot CuCO_3 \cdot Cu(OH)_2]$ are $\log K = 33.78$ and $\log K = 45.96$ at 25°C[26, 27].

The present results also reveal that the yield of soluble Cu(II) species can be strongly increased through stirring in solutions containing $NaHCO_3$. Then, the dissolution of the anodic layer can proceed through the following reactions:

$$[CuCO_3 \cdot Cu(OH)_2] + 3HCO_3^- = 2[Cu(CO_3)_2]^{2-} + 2H_2O + H^+, \quad (5a)$$

$$[CuCO_3 \cdot Cu(OH)_2] + HCO_3^- + H_2O = 2[CuCO_3(OH)_2]^{2-} + 3H^+, \quad (5b)$$

and

$$[Cu(OH)_2 \cdot 2CuCO_3] + 4HCO_3^- = 3[Cu(CO_3)_2]^{2-} + 2H_2O + 2H^+, \quad (6a)$$

$$[Cu(OH)_2 \cdot 2CuCO_3] + HCO_3^- + 4H_2O = 3[CuCO_3(OH)_2]^{2-} + 5H^+. \quad (6b)$$

The conclusive influence of HCO_3^- for destroying the anodic layer formed on Cu is observed for those specimens passivated in borate buffer (Figs 6 and 7). Reactions (5)–(6) imply the formation of Cu carbonate soluble complexes and simultaneous local acidification of the interface. The contribution of these reactions decreases as the pH of the solution is increased. Therefore, the cathodic baseline seen in the voltammogram can be explained as the electroreduction of the soluble Cu complexes formed through reactions (5)–(6).

The influence of ω on the anodic current read at $E = 0.45$ V can be clearly seen in Fig. 6. In this case, the quasi-steady current resulting at $\omega = 500$ rpm indicates that at this potential the electroformation and the chemical dissolution of the anodic layer happen at nearly equal rates. The anodic limiting current density, 8×10^{-4} A cm^{-2}, is equivalent to a Cu dissolution rate equal to 4.2×10^{-9} mol cm^{-2} s^{-1}. Accordingly, the residual anodic current resulting from the current transients provides an indication of the protective characteristics of the anodic layer formed on Cu in the different solutions at comparable pH and applied potential conditions. Thus, the residual anodic current read at 0.2 V decreases from 0.15 mA cm^{-2} for pH 8.8 to 0.087 mA cm^{-2} for pH 11.1. The preceding conclusions agree with those recently reported for the electrochemical behaviour of Cu in solutions containing $NaHCO_3$[20] in the 0.001–0.1 M range.

4.1. *The interpretation of anodic current transients*

The formation of the anodic layer on Cu in solutions containing $NaHCO_3 + Na_2CO_3$ can be interpreted in terms of nucleation and growth models applicable to the formation of new phases at the metal/solution interface[8, 15, 28, 29]. In the present work, the anodic current transients depend whether the electro-oxidation potential step covers the potential range of either peak I_a or peak II_a. In the former case the anodic layer grows either on base Cu or on a Cu surface covered by a $Cu(OH)_{ad}$ monolayer; whereas for the second case the Cu surface is already coated by a $Cu_2O/CuCO_3$ layer, and the anodic process leads to the thickening of the anodic layer. The apparent anodic current density, j_t, in both cases can be associated with several contributions, namely a term j_{dl} associated with the double layer charging; a term j_p related to the proper anodic layer growth; and a term j_d resulting from the balance of the metal dissolution through the anodic layer and the chemical dissolution of the anodic layer itself. Thus,

$$j_t = j_{dl} + j_p + j_d. \quad (7)$$

Under the present circumstances the double layer charging component quickly drops to zero in time, therefore, its contribution in equation (7) can be neglected. Then, equation (7) reduces to

$$j_t = j_p + j_d. \quad (8)$$

As a first approach one can also describe the growth of the anodic layer as an instantaneous nucleation and two-dimensional growth under diffusion control. The corresponding rate equation is[30]:

$$j_p = P_1 \exp(-P_2 t), \quad (9)$$

where

$$P_1 = q\pi KDN_0, \quad (9a)$$

$$P_2 = \pi KDN_0, \quad (9b)$$

$$P_1/P_2 = q, \quad (9c)$$

q is the charge density involved in the anodic layer formation, K is a proportionality constant, D is the diffusion coefficient of the species involved in the anodic layer growth and N_0 is the number of sites available for nucleation. It should be noted that a similar equation has been derived for multilayer growth by adsorption[31].

On the other hand, Cu electrodissolution can be assigned to the diffusion of Cu(II) ions from the metal surface through the anodic layer to the solution. For this process the equation is:

$$j_d = P_3 t^{-1/2}, \quad (10)$$

where

$$P_3 = zFD^{*1/2}\Delta c\pi^{-1/2}, \quad (10a)$$

and D^* has the same meaning as before, but applied to the conditions of the new process, and Δc is the concentration gradient associated with the Cu electrodissolution process through the anodic layer. The linear $\ln j_{p,II_a}$ vs. $\ln v$ relationships with slopes approaching 0.5 which were observed in this case, are consistent with a solid phase diffusion controlled Cu electrodissolution.

By using equations (8)–(10) the current transients recorded in the potential range of peak I_a (Fig. 8a)

and peak II_a (Fig. 8b) at different pH can be reproduced with the set of parameters assembled in Table 1. These parameters contain valuable information about the characteristics of the anodic processes.

The value of P_1 becomes nearly independent on the $NaHCO_3/Na_2CO_3$ concentration ratio; whereas P_2 depends on the solution composition, its lowest value resulting in 0.1 M $NaHCO_3$ (pH 8.8). This fact is consistent with the anodic layer dissolving properties of HCO_3^- ions. From $P_1/P_2 = q$, the charge density related to the anodic layer growth can be obtained. For the solutions containing Na_2CO_3 and $NaHCO_3 + Na_2CO_3$ the value of q approaches the $Cu(OH)_{ad}$ monolayer charge density ($q \cong 0.37\,mC\,cm^{-2}$)[32], whereas for solutions containing $NaHCO_3$, q is about twice. The same figure can be also derived from the voltammetric charge density related to peak I_a. Therefore, it is reasonable to admit that the charge density involved in j_p corresponds only to that required for the building up the inner Cu_2O layer. These results are coherent with the formation of $CuCO_3$ from the initial stages of the anodization process as referred to in the preceding section.

Otherwise, the value of P_3 increases with decreasing pH as one should expect for the HCO_3^- ion assisted dissolution of the anodic layer. Other comparable electrochemical systems such as the anodic layer formation on Cu in phosphate solutions[15] obey the same mechanism, but the presence of HCO_3^- ions in the solution increases considerably the value of P_3. Accordingly, the residual Cu electrodissolution current in $NaHCO_3$ solution becomes greater than in phosphate solution[15].

The physical picture involved in the preceding model can be summarized as follows. A small part of the anodic charge belongs to the inner Cu_2O passive layer. The accumulation of this charge occurs for $t < 5$ s and it can be associated with j_p. Another part of the anodic charge is related to a Cu electrodissolution process involving the diffusion of Cu(II) ions from the metal/inner oxide layer to the inner oxide layer/solution interface. This process is slow and can be associated with the term j_d. Besides, when the potential exceeds the potential range of peak II_a the anodic charge is used up in part to grow the outer $CuO/Cu(OH)_2$–$CuCO_3$ complex layer, and in part to form soluble Cu(II) species. However, equation (8) predicts a j vs. $t^{-1/2}$ law which for $t > 10$ s is not observed, as j_t becomes then practically constant. This apparent discrepancy can be explained considering that for $t \geqslant 5$ s, $j_p \geqslant 0$ and h, the layer thickness, becomes practically constant. Then, the diffusion layer thickness becomes equal to h and j_d becomes constant. This residual current can be interpreted as Cu corrosion current through a constant thickness $Cu_2O/CuO/Cu(OH)_2$–$CuCO_3$ layer.

4.2. *The interpretation of cathodic current transients*

In the presence of $NaHCO_3$ and Na_2CO_3 in the solution the anodic layers formed on Cu specimens can be described as a composed structure consisting of an inner Cu_2O–CuOH layer, and intermediate

Table 1. Parameters used for adjusting the Cu(O)/Cu(I) and Cu(I)/Cu(II) anodic current transients

Solution	E_c (V)	E_a (V)	$10^4 P_1$ ($A\,cm^{-2}$)	P_2 (s^{-1})	$10^4 P_3$ ($A\,s^{1/2}\,cm^{-2}$)
		First electro-oxidation stage			
0.1 M Na_2CO_3	−0.627	−0.305	13.7	20.2	3.19
		−0.250	17.6	13.0	3.57
		−0.205	36.5	10.4	2.49
0.05 M $NaHCO_3$ + 0.5 M Na_2CO_3	−0.650	−0.250	22.1	56.0	1.93
		−0.225	19.6	51.9	2.68
		−0.157	21.7	18.2	3.44
0.1 M $NaHCO_3$	−0.550	−0.130	17.7	2.95	14.1
		−0.160	16.8	1.97	9.23
		Second electro-oxidation stage			
0.1 M Na_2CO_3	−0.430	−0.110	17.6	195	0.87
		−0.073	5.13	331	1.61
		−0.055	2.66	13.5	2.00
		−0.035	9.67	9.70	1.76
		0.010	31.1	21.2	2.54
		0.250	130	37.3	7.02
0.5 M $NaHCO_3$ + 0.5 M Na_2CO_3	−0.423	0.020	28.6	34.5	3.30
		0.035	36.7	27.7	2.97
		0.060	44.1	27.3	3.38
		0.305	151	30.8	3.64
0.1 M $NaHCO_3$	−0.241	0.045	57.9	30.7	1.49
		0.082	8.03	6.67	0.58
		0.105	7.91	10.1	1.01
		0.200	19.2	17.4	1.26
	−0.350	0.016	2.00	5.85	0.99
		0.041	5.38	10.1	1.15
		0.105	13.8	17.9	1.46
		0.300	63.7	29.7	2.04

CuO–$Cu(OH)_2$ layer, an outer $Cu(OH)_2$–$CuCO_3$ layer, the stoichiometry of the latter depending on the pH of the solution[2].

The electroreduction of the Cu(II) layers to Cu_2O (or CuOH) would proceed through the following global reaction:

$$CuCO_3\text{–}Cu(OH)_2 \text{ layer} + 2e^- = Cu_2O + H_2O + CO_3^{2-}, \quad (11)$$

which implies a solid phase change. The latter is likely responsible for the sharp peak II_c' appearing in the complex structure of peak II_c. A process comparable to that represented by equation (11) has been earlier described for the electroreduction of $Cu(OH)_2$ layers in plain NaOH solutions[9].

The intermediate CuO–$Cu(OH)_2$ layer can be also electroreduced to Cu_2O according to global processes such as:

$$2CuO + HCO_3^- + 2e^- = Cu_2O + CO_3^{2-} + OH^-, \quad (12a)$$

$$2Cu(OH)_2 + HCO_3^- + 2e^- = Cu_2O + CO_3^{2-} + OH^- + 2H_2O, \quad (12b)$$

and

$$2Cu(OH)_2 + 2e^- = Cu_2O + H_2O + 2OH^-, \quad (13a)$$

$$2CuO + H_2O + 2e^- = Cu_2O + 2OH^-. \quad (13b)$$

At high cathodic potentials ($E < E_r$) the electroreduction to Cu(O) can be related to the appearance of peak I_c and the corresponding global reactions can be represented as follows:

$$Cu_2O + H_2O + 2e^- = 2Cu + 2OH^-, \quad (14a)$$

and

$$Cu(OH)_2 + 2e^- = Cu + 2OH^-. \quad (14b)$$

At present the analysis of the cathodic current transients obtained at constant potential offers the possibility of modeling only the potentiostatic electroreduction of the Cu(II) anodic layers to Cu_2O (peak II_c). The voltammograms related to this process are rather complex and revealed that several contributions are involved when the reaction proceeds in the potential range of peak II_c. Furthermore, the pH dependence of the potential of peak II_c is greater than that expected for a reversible electrochemical reaction [see section 3.1.1]. The same conclusion about the complexity of the electroreduction processes can be derived from the shape of the potentiostatic current transients (Fig. 9).

As a first approach the potentiostatic electroreduction current transients can be modeled considering three main contributions:

$$j_{cII} = j_{cd} + j_{cn} + j_r, \quad (15)$$

where j_{cII} is the total cathodic current density involved in the electroreduction process; j_{cd} is a diffusion controlled current density which is associated with the fast initial current decay; j_{cn} is a current density producing a maximum current value in the transient, which can be related to the nucleation and growth of a new phase in the passive layer; and j_r can be assigned to the electrodeposition current of residual soluble Cu(II) species. Thus, j_r is given by:

$$j_r = P_4, \quad (16)$$

and j_{cd} can be expressed:

$$j_{cd} = P_5 t^{-1/2}, \quad (17)$$

where

$$P_5 = zFD^{\#\,1/2}\Delta c^{\#}\pi^{-1/2} \quad (17a)$$

$D^{\#}$ and $\Delta c^{\#}$ are assigned to the diffusion coefficient and the concentration gradient of species entering the first electroreduction stage [reactions (13a) and (13b)].

On the other hand, the term j_{cn} can be linked to the nucleation and two-dimensional growth of a new phase under charge transfer control [reaction (13)]. This assumption can be justified through the linear $\ln j_{M,IIc}$ vs. E_s plot approaching the slope $2RT/F$ (Fig. 10). Thence, the corresponding current transient equations for an instantaneous nucleation are[33]:

$$j_{cn} = P_6 t \exp(-P_7 t^2), \quad (18)$$

where

$$P_6 = 2zF\pi MhN_0 k^2 \rho^{-1}, \quad (18a)$$

$$P_7 = \pi M^2 N_0 k^2 \rho^{-2}, \quad (18b)$$

and for a progressive nucleation is:

$$j_{cn} = P_8 t^2 \exp(-P_9 t^3), \quad (19)$$

with

$$P_8 = 2F\pi MhAk^2\rho^{-1}, \quad (19a)$$

$$P_9 = \pi M^2 Ak^2(3\rho^2)^{-1}. \quad (19b)$$

A is the nucleation rate, k is the growth rate constant, ρ is the specific gravity and M is the molecular weight of the electroreduced species.

By using equations (16), (17) and (19) at low cathodic potentials, and equations (16)–(18) at high cathodic potentials, the current transients recorded in solutions containing Na_2CO_3 and $NaHCO_3$ can be reproduced with the parameters assembled in Table 2.

According to data shown in Table 2, at low cathodic potentials the Cu(II)/Cu(I) electrochemical phase change can be described through the formalism of a progressive nucleation and a two-dimensional phase growth mechanism; whereas at high cathodic potentials the process likely occurs through an instantaneous nucleation and a two-dimensional phase change mechanism. These conclusions agree with the SEM micrographs resulting from the electroreduction process showing patches where the reaction takes place rather uniformly distributed on the electrode surface (Fig. 11).

At a constant solution composition the value of P_5 slightly increases as the value of E_s is negatively increased. This trend, observed under different experimental conditions, may be assigned to either an increase of $\Delta c^{\#}$ with E_s or an electric field-assisted transport of reaction products at the reaction layer. It should be noted that the charge density contribution related to P_5 is equivalent to about two monolayers of reactant.

Table 2. Parameters used for adjusting the Cu(II)/Cu(I) cathodic current transients

E_a (V)	t_a (s)	E_s (V)	$10^4 P_5$ ($A s^{1/2} cm^{-2}$)	$10^4 P_6$ ($A s^{-1} cm^{-2}$)	P_7 (s^{-2})	$10^4 P_8$ ($A s^{-2} cm^{-2}$)	P_9 (s^{-3})
			0.1 M Na_2CO_3				
0	50	−0.200	0.52	—	—	0.26	0.033
		−0.250	1.03	—	—	8.48	1.84
		−0.300	1.24	21.4	7.62	—	—
0.010	100	−0.196	0.305	—	—	0.21	0.022
		−0.245	0.589	6.50	0.88	—	—
0.250	100	−0.340	2.26	13.6	1.28	—	—
			0.05 M $NaHCO_3$ + 0.05 M Na_2CO_3				
0.063	100	−0.150	0.23	—	—	1.14	0.099
		−0.185	0.38	—	—	1.14	1.11
		−0.300	1.79	187	38.5	—	—
0.304	100	−0.173	0.73	—	—	0.013	0.014
		−0.192	0.92	—	—	0.12	0.005
		−0.217	1.02	—	—	1.71	0.085
		−0.325	2.88	126	12.5	—	—
			0.1 M $NaHCO_3$				
0.104	50	−0.151	0.14	—	—	1.28	0.546
		−0.190	0.29	10.3	4.12	—	—
		−0.241	0.67	37.6	18.7	—	—
	100	−0.150	0.14	—	—	0.89	0.28
		−0.190	0.26	9.74	2.83	—	—
		−0.241	0.67	33.1	15.0	—	—
0.106	100	−0.135	0.30	—	—	0.19	0.026
		−0.150	0.14	—	—	1.72	0.297
		−0.180	0.36	—	—	20.7	4.65
		−0.300	1.49	223	89.3	—	—
0.122	100	−0.130	0.36	—	—	0.276	0.034
		−0.160	0.44	—	—	1.70	0.23
		−0.230	0.873	28.5	6.43	—	—
0.250	100	−0.155	0.937	—	—	1.09	0.11
		−0.175	1.02	—	—	5.24	0.55
		−0.239	1.48	43.7	6.45	—	—
0.495	100	−0.180	0.636	—	—	0.021	0.00075
		−0.213	0.877	—	—	0.318	0.0143
		−0.280	1.46	11.1	0.72	—	—

On the other hand, the values of P_6 and P_8 and P_7 and P_9 also depend on E_s. The potential dependence of these parameters should be principally assigned to the potential dependence of the corresponding k values. Accordingly, the increase of those parameters with E_s would reflect the slowness of the process through the number of nucleation centers as expected from equations (19) and (20). Let us assume that under a particular set of experimental conditions, the potential dependence of the values, k for the instantaneous nucleation, and the product kA for the progressive nucleation, is given by a Tafel-type relationship with a transfer coefficient equal to 0.5, *ie* $(\Delta \ln k/\Delta E_s) = 2RT/F$. For this case, the slopes of the $\ln P_i$ ($i = 6, 7, 8, 9$) vs. E_s plots should approach the slope RT/F. Despite data scattering, for constant solution composition and electrochemical routine conditions, the trend to approach the linear slope RT/F is observed. For the cathodic process, the results are consistent with the potential dependence of $j_{M,IIc}$ as shown in Fig. 10.

Finally, the constant term j_r comprises the electrodeposition current of residual Cu(II) soluble species, and the magnitude of this contribution changes between 0.2×10^{-4} and 0.5×10^{-4} A cm^{-2}, depending on the history of each run.

5. CONCLUSIONS

(i) The anodic layers formed on Cu in $NaHCO_3$ + Na_2CO_3 solutions can be described as composed layers involving an inner Cu_2O and an outer $CuO/Cu(OH)_2$–$CuCO_3$ complex layer. The relative amount of material related to these layers depends on pH, potential and anodization time. Cathodic processes comprise the electroreduction of the anodic layer and the electrodeposition of soluble Cu(II) species.

(ii) Solution stirring hinders the formation of the anodic layer and increases the yielding of soluble Cu(II) species.

(iii) The appearance of soluble species can be explained through a complexation of Cu(II) at the anodic layer by HCO_3^- ions.

(iv) The anodic current transients related to the electroformation of the anodic layer and to Cu electrodissolution can be reproduced by using a model for the nucleation and growth of new phases under diffusion control. The cathodic current transients related to the first electroreduction stage of the anodic layer can be mainly described in terms of a nucleation and growth model under activation control.

(v) In $NaHCO_3 + Na_2CO_3$ solutions the passivity of Cu is less effective than in either phosphate, borate or plain NaOH solutions.

Acknowledgement—Financial support for this work by the Gobierno de Canarias (Dirección General de Universidades e Investigación) under contract No. 46/01.06.88, is gratefully acknowledged.

REFERENCES

1. U. Bertocci and D. Turner, in *Encyclopedia of Electrochemistry of the Elements* (Edited by A. J. Bard), Vol. 2. Marcel Dekker, New York (1974).
2. J. van Muylder, in *Comprehensive Treatise of Electrochemistry* (Edited by J. O'M. Bockris, B. E. Conway, E. Yeager and R. White), Vol. 4, p. 23. Plenum Press, New York (1981).
3. D. W. Shoesmith, T. E. Rummery, D. Owen and W. Lee, *J. electrochem. Soc.* **123,** 790 (1976).
4. W. Ashworth and D. Fairhust, *J. electrochem. Soc.* **123,** 506 (1977).
5. H. H. Strehblow and H. D. Speckmann, *Werkstoffe Korros.* **35,** 512 (1984).
6. M. R. G. de Chialvo, S. L. Marchiano and A. J. Arvia, *J. appl. Electrochem.* **14,** 165 (1984).
7. H. D. Speckmann, M. M. Lohrengel, J. W. Schultze and H. H. Strehblow, *Ber. Bunsenges. Phys. Chem.* **89,** 392 (1985).
8. M. R. G. de Chialvo, R. C. Salvarezza, D. V. Vásquez Moll and A. J. Arvia, *Electrochim. Acta* **30,** 1501 (1985).
9. J. Gómez Becerra, R. C. Salvarezza and A. J. Arvia, *Electrochim. Acta* **33,** 613 (1988).
10. S. Dong, Y. Xie and G. Cheng, *Electrochim. Acta* **37,** 17 (1992).
11. M. R. G. de Chialvo, J. O. Zerbino, S. L. Marchiano and A. J. Arvia, *J. appl. Electrochem.* **16,** 517 (1986).
12. M. Wanner, H. Wiese and K. G. Weil, *Ber. Bunsenges. Phys. Chem.* **92,** 736 (1988).
13. M. Pérez Sánchez, M. Barrera, S. González, R. M. Souto, R. C. Salvarezza and A. J. Arvia, *Electrochim. Acta* **35,** 1337 (1990).
14. C. I. Elsner, R. C. Salvarezza and A. J. Arvia, *Electrochim. Acta* **33,** 1735 (1988).
15. M. M. Laz, R. M. Souto, S. González, R. C. Salvarezza and A. J. Arvia, *Electrochim. Acta* **37,** 655 (1992).
16. D. Vásquez Moll, M. R. G. de Chialvo, R. C. Salvarezza and A. J. Arvia, *Electrochim. Acta* **30,** 1011 (1985).
17. M. G. Figueroa, M. F. L. de Mele, R. C. Salvarezza and A. J. Arvia, *Electrochim. Acta* **32,** 231 (1987).
18. M. R. G. de Chialvo, M. F. L. de Mele, R. C. Salvarezza and A. J. Arvia, *Corros. Sci.* **28,** 121 (1988).
19. R. M. Souto, M. Pérez Sánchez, M. Barrera, S. González, R. C. Salvarezza and A. J. Arvia, *Electrochim. Acta* **37,** 1437 (1992).
20. M. Drogowska, R. L. Brossard and H. Ménard, 42nd. Meeting of the International Society of Electrochemistry, Montreux, 25–30 August, 1991, paper 4–15, *J. electrochem. Soc.* **139,** 39 (1992).
21. D. Dickertmann, F. D. Koppitz and J. W. Schultze, *Electrochim. Acta* **21,** 967 (1976).
22. B. D. Cahan and H. M. Villullas, *J. electroanal. Chem.* **307,** 263 (1991).
23. A. M. Castro Luna, S. L. Marchiano and A. J. Arvia, *J. appl. Electrochem.* **8,** 121 (1978).
24. S. L. Marchiano, C. I. Elsner and A. J. Arvia, *J. appl. Electrochem.* **10,** 365 (1980).
25. S. T. Mayer and R. H. Muller, *J. electrochem. Soc.* **139,** 426 (1992).
26. R. M. Smith, A. E. Martell, *Critical Stability Constants* Vol. 4. Pergamon Press, New York (1976).
27. J. W. Mellor, *A Comprehensive Treatise on Inorganic and Theoretical Chemistry,* Vol. 3, p. 276. Longmans, Green, London (1928).
27. R. C. Salvarezza, D. V. Vásquez Moll and A. J. Arvia, *Electrochim. Acta* **32,** 1421 (1987).
28. R. C. Salvarezza, D. V. Vásquez Moll and A. J. Arvia, *Electrochim. Acta* **32,** 1421 (1987).
29. D. V. Vásquez Moll, R. C. Salvarezza, H. Videla and A. J. Arvia, *J. electrochem. Soc.* **132,** 754 (1985).
30. W. Davison and J. A. Harrison, *J. electroanal. Chem.* **44,** 213 (1973).
31. R. G. Barradas and E. Bosco, *J. electroanal. Chem.* **193,** 23 (1985).
32. M. E. Garmanov, S. G. Prutchenko, A. S. Sadovskii and V. A. Makarov, *Elektrokhimiya* **24,** 1035 (1988).
33. M. Fleischmann and H. R. Thirsk, in *Advances in Electrochemistry and Electrochemical Engineering* (Edited by P. Delahay), Vol. 3, p. 123. Interscience, New York (1961).